NANO LETTERS

2009
Vol. 9, No. 8
2991-2995

Nonlinear Optical Imaging of Individual Carbon Nanotubes with Four-Wave-Mixing Microscopy

Hyunmin Kim,[†] Tatyana Sheps,[‡] Philip G. Collins,*[,‡] and Eric O. Potma*[,†]

Department of Chemistry, University of California, Irvine, California 92697-2025, and Department of Physics and Astronomy, University of California, Irvine, California 92697-4576

Received May 4, 2009; Revised Manuscript Received July 13, 2009

ABSTRACT

Dual color four-wave-mixing (FWM) microscopy is used to spatially resolve the third-order optical response from individual carbon nanotubes. Good signal-to-noise is obtained from single-walled carbon nanotubes (SWNT) sitting on substrates, when the excitation beams are resonant with electronic transitions of the nanotube, by detecting the FWM response at the anti-Stokes frequency. Whereas the coherent anti-Stokes (CAS) signal is sensitive to both electronic and vibrational resonances of the material, it is shown that the signal from individual SWNTs is dominated by the electronic response. The CAS signal is strongly polarization dependent, with the highest signals found parallel with the enhanced electronic polarizibility along the long axis of the SWNT.

The quasi-one-dimensional structure of single-walled carbon nanotubes (SWNTs) dresses these nanosystems with electronic properties that are absent in bulk metallic and semiconductor materials.[1] A clear understanding of the unique electronic structure and the dynamics of electronic excitations in SWNTs is essential for optimizing the potential applications of carbon nanotubes. However, the rich structural diversity of SWNTs in standard preparations, which produces a broad variation of electronic properties in the ensemble, makes a direct comparison between theories of electronic structure and experiment rather challenging. Optical examination of individual SWNTs avoids the heterogeneity of ensemble preparations, and constitutes a powerful approach to probe electronic properties in great detail. For instance, fluorescence microscopy was instrumental in the observation of different structural order in a single SWNT,[2] and Raman microspectroscopy has been successfully utilized to connect structure to collective bond vibrations.[3] Moreover, direct information on the transition energies in metallic and semiconducting SWNTs was obtained with the Rayleigh scattering technique on individual, suspended SWNTs.[4] By combining Rayleigh scattering with electron microscopy, direct assignments of optical transitions have been made for a variety of SWNTs of defined chirality.[5]

None of these optical techniques, however, provide time-resolved measurements of carrier dynamics, and therefore the connections between these dynamics and electronic structure have not been addressed with single SWNT specificity. Time-resolved nonlinear spectroscopic techniques are capable of probing both the incoherent interstate relaxation mechanisms as well as the coherent coupling between states and the associated dephasing processes, providing a detailed picture of excited state dynamics. For instance, ensemble pump−probe experiments have revealed the time scales of inter- and intraband relaxation dynamics and lifetimes of the excitonic states.[6−9] Ultrafast optical experiments have also uncovered the coherent[10] and incoherent[11] relaxation of vibrational modes that are coupled to the electronic transitions. Whereas nonlinear spectroscopic experiments have provided important insight into the electronic and vibrational response of nanotubes on the ensemble level, probing the structure-specific dynamics of optical excitations ultimately depends on the ability to detect the coherent and incoherent nonlinear response of individual SWNTs. However, low optical signal yields have hitherto precluded a direct recording of the time-resolved nonlinear response of SWNTs on a single nanotube level.

In this work, we demonstrate a new optical microscopy of individual SWNTs using a nonlinear, coherent, four-wave-mixing (FWM) technique. An ultrafast pump (ω_p) and Stokes (ω_S) pulse pair excites the SWNT, and radiation from third-order electronic coherences is detected at the anti-Stokes frequency ($2\omega_p - \omega_S$) as depicted in Figure 1.[12] Unlike stimulated parametric emission (SPE) microscopy,[13] this coherent anti-Stokes (CAS) form of FWM microscopy is

* Corresponding authors, collinsp@uci.edu and epotma@uci.edu.
[†] Department of Chemistry.
[‡] Department of Physics and Astronomy.

10.1021/nl901412x CCC: $40.75
Published on Web 07/28/2009

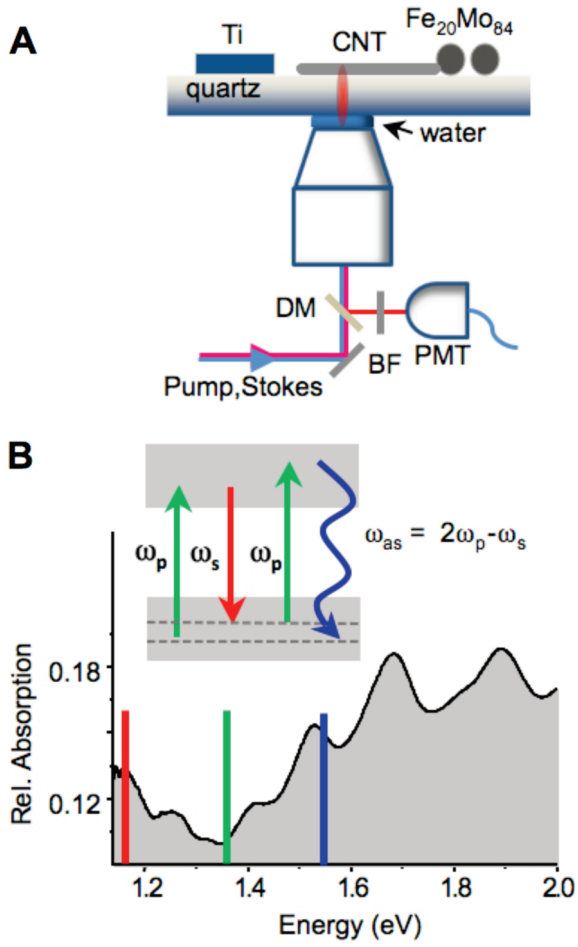

Figure 1. (A) Experimental setup: DM, dichroic mirror; BF, bandpass filter; PMT, photomultiplier tube. (B) Energy diagram for coherent anti-Stokes scattering (CAS). Cartoon of the excitation energies of pump, Stokes and anti-Stokes relative to the absorption spectrum of a SWNT ensemble (from ref 8).

enhanced by one-photon resonances and is a sensitive probe for the nonlinear electronic response of nanoscale objects.[12,14] Strong CAS signals are expected when the excitation energies overlap with electronic excitation energies of the SWNT. The ability to detect coherent nonlinear signals from individual nanotubes opens up opportunities for time-resolved optical investigations on the single SWNT level.

Experiments are primarily performed on small diameter SWNTs grown by catalyst-assisted chemical vapor deposition (CVD) of methane, following the techniques of Liu et al.[15] except with the use of 4 in. single crystal quartz wafers (*c*-axis). The molecular catalyst produces SWNTs with a diameter range of 0.9−1.4 nm when highly diluted, and larger diameter SWNTs and multiwalled nanotubes (MWNTs) when it is allowed to aggregate. After growth, multiple Ti electrodes are patterned by optical lithography and deposited on top of the SWNTs by electron beam evaporation to make electrical contacts. The electrodes are approximately 30 nm high, with a minimum separation of 2.0 μm. SWNTs are located and characterized by electrical measurements, scanning electron microscopy (SEM), and atomic force microscopy (AFM) before and after the optical measurements.

Optical imaging is performed in a laser-scanning microscope system configured for coherent anti-Stokes Raman scattering (CARS) microscopy, as depicted in Figure 1A.[16] We employ 7 ps pulse trains (76 MHz repetition rate) derived from a synchronously pumped optical parametric oscillator system. Although higher excitation efficiencies are expected for broad band femtosecond pulses, we use narrowband excitation in this study to increase the spectral selectivity for vibrational signatures. The Stokes beam is fixed at 1.16 eV, whereas the pump beam can be varied between 1.55 and 1.35 eV, and both excitation powers are kept below 2 mW. As shown in Figure 1B, the excitation energies show appreciable overlap with the transition energies of a similar SWNT ensemble.[8] The beams are focused to a submicrometer sized focal spot by a 40×, 1.15 NA water immersed objective lens, and imaging is performed directly through the quartz wafer in the inverted microscope configuration. Signals are collected in the epi-direction at a pixel dwell time of 22.5 μs. Signals were averaged 50 times to achieve the signal-to-noise required for resolving an isolated SWNT, amounting to a total signal integration time of 1.13 ms per pixel. Unless noted otherwise, all images are collected at zero time delay between the pump and the Stokes pulses.

Figure 2 shows representative imaging results for a SWNT. The CAS image in Figure 2A clearly resolves the SWNT, with an apparent width set by the ~0.5 μm lateral resolution of the nonlinear optical microscope. In the chosen range of the excitation energy, no background luminescence was observed from the nanotubes at the anti-Stokes frequency. The CAS signal disappears whenever the pump and probe pulses are temporally detuned. The corresponding SEM image is given in Figure 2B. An AFM topographic analysis indicates a SWNT diameter of 1.0 nm. In this example, AFM analysis is performed after the CAS imaging to confirm the absence of obvious photodamage to the SWNT. A comparison of SEM and CAS images reveals furthermore that CAS only resolves a subset of the SWNTs present on a substrate. Independent electrical measurements revealed that detectable CAS signals were observed from metallic nanotubes. Semiconducting SWNTs have not yet been successfully imaged at the particular excitation energies typically used here (pump 1.36 eV and Stokes 1.17 eV). Therefore, the remaining results and discussion below pertain only to metallic SWNT and MWNT samples.

Figure 2C depicts the dependence of the CAS signal on carbon nanotube diameter. While the CAS signal intensity is highly variable from one nanotube to the next, a comparison with AFM topography indicates that most of this variation correlates with outer diameter. In fact, the intensity can be fitted to a function that approximates the square of the number of carbon atoms in the focal area. In contrast, in the case of incoherent Raman scattering, the signal scales linearly with the number of carbon atoms.[17] The square dependence of the CAS intensity on the number of carbon atoms, and accordingly the number of π-electrons, provides evidence for the coherent nature of the nonlinear CAS signal.

The CAS imaging demonstrated in Figure 2A is sensitive to beam polarization, and maximum signals are obtained

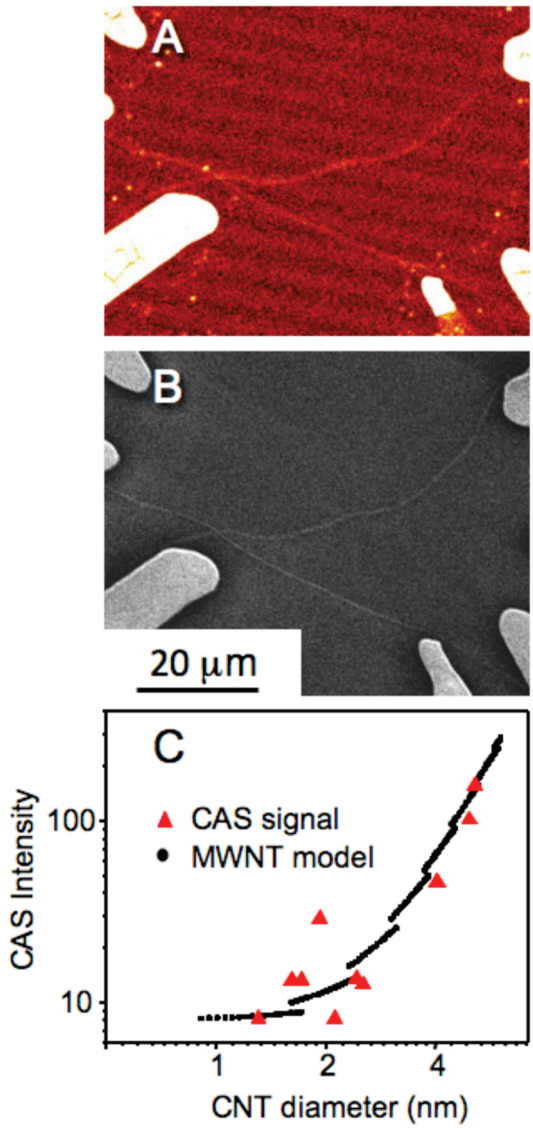

Figure 2. (A) CAS image of two SWNTs of diameter 1.0 nm. Pump was 1.0 mW at 1.36 eV and Stokes was 2.0 mW at 1.16 eV. (B) SEM image of the same area. (C) CAS signal as a function of nanotube diameter. Black circles indicate a model of the CAS intensity (I) having the form $I = \text{offset} + (aN)^2$ where a is a scaling constant and N comes from a simple model estimating the total number of carbon atoms in a nanotube of known diameter. Steps in the model result at each diameter where MWNTs likely gain additional carbon layers.

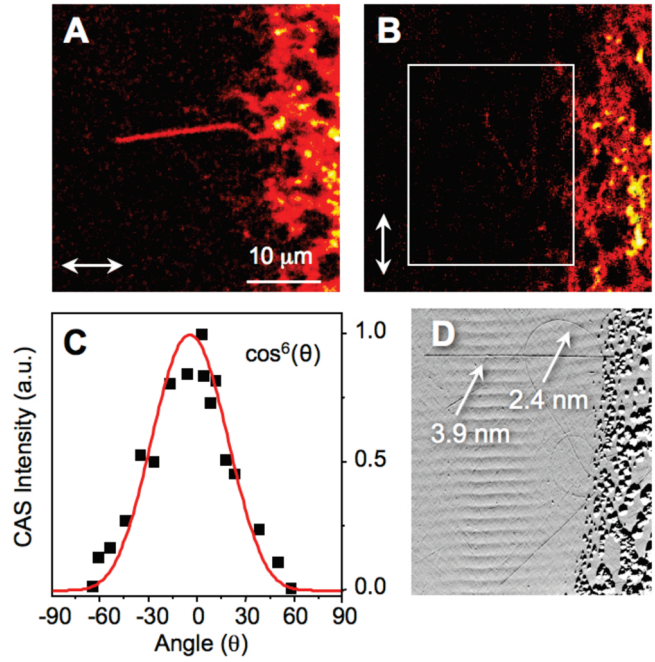

Figure 3. CAS image of an individual CNT when the polarization of the incident beam is (A) parallel and (B) perpendicular to the long axis of the nanotube. (C) CAS intensity as a function of the angle of between the beam polarization and the long axis of the CNT. (D) AFM image of the area marked by white square in panel B. CNT diameters as determined from topographic analysis are indicated.

when a SWNT is aligned with the excitation fields. This effect is demonstrated in Figure 3, where a small number of crossing MWNTs vary from visible to invisible as the excitation polarization is rotated. In Figure 3A, a straight MWNT with a diameter of 3.9 nm is clearly imaged by an excitation field aligned parallel to it. Upon rotation of the polarization by 90 , this MWNT vanishes and neighboring MWNTs better aligned with the fields become visible (Figure 3B). Similar effects are observed with SWNTs, but the much stronger CAS intensity from MWNTs allows the exact angle dependence to be more accurately determined. As shown in Figure 3C, the CAS intensity follows a $\cos^6 \theta$ dependence, where θ is defined as the angle between the long axis of the MWNT and the beam polarization. This dependence confirms that the response scales to the third order with the incoming excitation intensity. It also shows that the excitations involved in the CAS mechanism are strongly enhanced in this longitudinal direction.

To further distinguish between electronic and vibrational excitations as the responsible mechanism for the experimental CAS signal, we have chosen a pump energy close to 1.36 eV such that the energy difference between the pump and Stokes may be tuned in and out of resonance with the vibrational energy of the G-mode of the carbon lattice near 1580 cm^{-1}. With the energy difference between the pump and Stokes beams set to 1596 cm^{-1}, Figure 4A shows a MWNT (arrow 1), in addition to a region that predominantly contains clumped graphitic material (arrow 2). When the energy difference is changed to 1578 cm^{-1}, the signal from the graphitic cluster has grown, whereas the signal from the MWNT has remained relatively constant (Figure 4B). The spectral dependence of these regions of interest is plotted in Figure 4C. A clear G-mode resonance is seen in the graphitic cluster, on top of an electronic background. This indicates that both electronic (CAS) and vibrational (CARS) resonances are probed in this form of imaging. The signal from the MWNT, however, is mainly electronic in nature. We propose that the gradual increase of the signal toward higher energies is attributed to the higher excitation energy of the pump beam probing the shape of the MWNT's excitation spectrum.

Whereas the carbon atom density in the MWNT is much lower than that in the graphite cluster, the electronic signal from both structures is comparable. The relatively strong

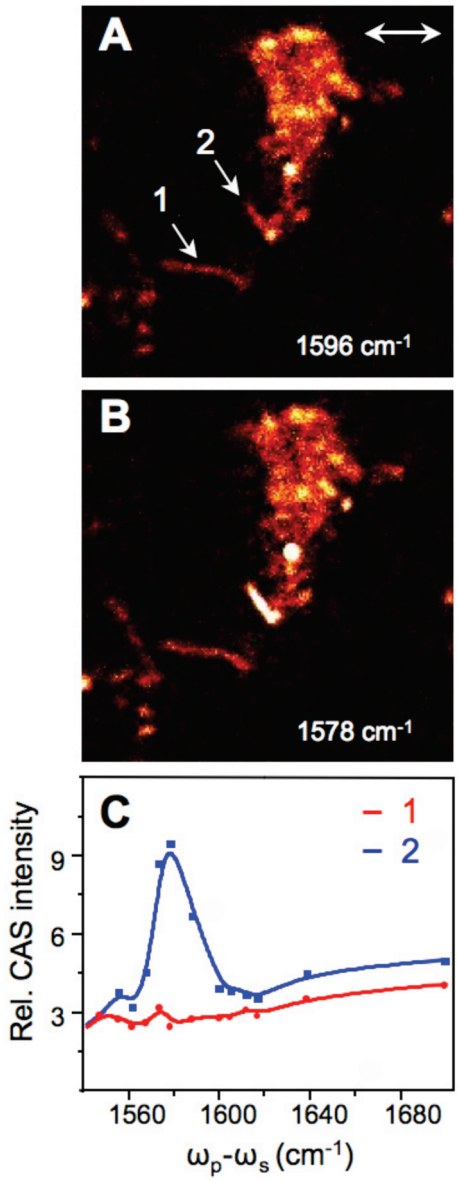

Figure 4. Spectral dependence of coherent anti-Stokes emission. (A) CAS image at $\omega_p - \omega_s = 1596$ cm^{-1}. The marked points correspond to a single nanotube (1) and a graphite cluster (2). The double arrow indicates the beam polarization. (B) CAS image at $\omega_p - \omega_s = 1578$ cm^{-1}. (C) CAS intensity as a function of $\omega_p - \omega_s$. Both vibrational and electronic components are seen in the cluster, whereas the CNT four-wave-mixing response is predominantly electronic.

response of the MWNT is a manifestation of the enhanced electronic properties along the long axis of the structure. A similar enhancement of the vibrational response is not observed in the MWNT, indicating that the coupling of the G-mode to the electronic excitation is relatively weak.

This work demonstrates that CAS imaging enables a careful examination of the nonlinear optical properties of individual SWNTs. The CAS response is particularly sensitive to electronic transitions, and detectable CAS signals are obtained from SWNTs that exhibit strong electronic transitions near the excitation energies used in this study (~1.2−1.5 eV). We believe that the imaging experiments reported here are sensitive to only a subset of SWNTs within the heterogeneous sample because the energy and nature of electronic transitions depend on SWNT chirality, diameter, and length.[18]

Similar to Rayleigh scattering, the CAS response should be enhanced by the electronic transitions in both metallic and semiconducting SWNTs. In this study, strongest CAS signals were obtained from metallic SWNTs, whereas insufficient signal-to-noise was achieved when imaging semiconducting SWNTs. A simple interpretation might be that the polarizibility of the semiconducting SWNTs is insufficient to generate detectable signals at the excitation energies employed in this study. Further work is required to determine the full spectral range of possible CAS responses.

Because the CAS signal is generated at the anti-Stokes frequency, it is insensitive to scattered contributions of the incident laser beams. Without background scattering contributions, detection of individual SWNTs becomes possible on a crystal quartz surface, even in the presence of highly scattering nanocatalyst particles and nearby electrodes. These flexible imaging conditions make CAS an attractive research tool for a broad range of carbon nanotube sample preparations. An important advantage of CAS imaging is that contrast is derived from the nonlinear optical response of the SWNT, as opposed to the linear optical properties measured in Rayleigh scattering and related techniques. Time-resolved variations of the four-wave-mixing experiment discussed in this paper are sensitive to the ultrafast dynamics of the excited electronic states and hold promise as sensitive probes for the exciton dynamics on a single molecule level. In addition, under conditions of a fast electronic response, time-resolved coherent anti-Stokes measurements are expected to enable a direct recording of the ground state vibrational dynamics of individual carbon nanotubes.

Acknowledgment. We thank Professor Ara Apkarian for useful discussions and A. A. Kane and D. Wan for help with sample preparation. This work was funded by the NSF Center on Chemistry at the Space-Time Limit at UCI (CHE-0533162). T.S. acknowledges support of a GAANN fellowship, and EOP acknowledges support from the American Chemical Society (PRF 46067-G6).

References

(1) Saito, R.; Dresselhaus, G. Dresselhaus, M. S. *Physical Properties of Carbon Nanotubes*; Imperial Press: London, 1998.
(2) Lefebvre, J.; Austing, D. G.; Bond, J.; Finnie, P. Photoluminescence imaging of suspended single-walled carbon nanotubes. *Nano Lett.* **2006**, *6*, 1603–1608.
(3) Hartschuh, A.; Pedrosa, H. N.; Novotny, L.; Krauss, T. D. Simultaneous fluorescence and Raman scattering from single carbon nanotubes. *Science* **2003**, *301*, 1354–1356.
(4) Sfeir, M.; Wang, F.; Huang, L.; Chuang, C. C.; Hone, J.; O'Brien, S. P.; Heinz, T. F.; Brus, L. E. Probing electronic transitions in individual carbon nanotubes by Rayleigh scattering. *Science* **2004**, *306*, 1540–1543.
(5) Sfeir, M. Y.; Beetz, T.; Wang, F.; Huang, L.; Huang, X. M. H.; Huang, M.; Hone, J.; Misewich, J. A.; Heinz, T. F.; Wu, L.; Zhu, Y.; Brus, L. E. Optical spectroscopy of individual single-walled carbon nanotubes of defined chiral structure. *Science* **2006**, *312*, 554–556.
(6) Lauret, J. S.; Voisin, C.; Cassabois, G.; Delalande, C.; Roussignol, P.; Jost, O.; Capes, L. Ultrafast carrier dynamics in single-wall carbon nanotubes. *Phys. Rev. Lett.* **2003**, *90*, 057404.
(7) Manzoni, C.; Gambetta, A.; Menna, E.; Meneghetti, M.; Lanzani, G.; Cerullo, G. Intersubband exciton relaxation dynamics in single-walled carbon nanotubes. *Phys. Rev. Lett.* **2005**, *94*, 207401.

(8) Seferyan, H. Y.; Nasr, M. B.; Senekerimyam, V.; Zadoyan, R.; Collins, P.; Apkarian, V. A. Transient grating measurements of excitonic dynamics in single walled carbon nanotubes: The dark excitonic bottleneck. *Nano Lett.* **2006**, *6*, 1757–1760.
(9) Huang, L. B.; Pedrosa, H. N.; Krauss, T. D. Ultrafast ground-state recovery of single-walled carbon nanotubes. *Phys. Rev. Lett.* **2004**, *93*, 017403.
(10) Lim, Y. S.; Yee, K. J.; Kim, J. H.; Hároz, E. H.; Shaver, J.; Kono, J.; Doorn, S. K.; Hauge, R. H.; Smalley, R. E. Coherent lattice vibrations in single-walled carbon nanotubes. *Nano Lett.* **2006**, *6*, 2696–2700.
(11) Song, D.; Wang, F.; Dukovic, G.; Zheng, M.; Semke, E. D.; Brus, L. E.; Heinz, T. F. Direct measurement of the lifetime of optical photons in single-walled carbon nanotubes. *Phys. Rev. Lett.* **2008**, *100*, 225503.
(12) Kim, H.; Taggart, D. K.; Xiang, C.; Penner, R. M.; Potma, E. O. Spatial control of coherent anti-Stokes emission with height-modulated gold zig-zag nanowires. *Nano Lett.* **2008**, *8*, 2373–2377.
(13) Isobe, K.; Kataoka, S.; Mutase, R.; Watanabe, W.; Higashi, T.; Kawakami, S.; Matsunaga, S.; Fukui, K.; Itoh, K. Stimulated parametric emission microscopt. *Opt. Express* **2006**, *12*, 11204–11214.
(14) Jung, Y.; Chen, H.; Tong, L.; Cheng, J. X. Imaging gold nanorods by plasmon-resonance-enhanced four wave mixing. *J. Phys. Chem. C* **2009**, *113*, 2657–2663.
(15) An, L.; Owens, J. M.; McNeil, L. E.; Liu, J. Synthesis of nearly uniform single-walled carbon nanotubes using identical metal-containing molecular nanoclusters as catalysts. *J. Am. Chem. Soc.* **2002**, *124*, 13688–13689.
(16) Zimmerley, M.; McClure, R. A.; Choi, B.; Potma, E. O. Following dimethyl sulfoxide skin optical clearing with quantitative nonlinear mulimodal microscopy. *Appl. Opt.* **2009**, *48*, D79–D87.
(17) Mews, A.; Koberling, F.; Basché, T.; Philipp, G.; Duesberg, G. S.; Roth, S.; Burghard, M. Raman imaging of single carbon nanotubes. *Adv. Mater.* **2000**, *12*, 1210–1214.
(18) Spataru, C. D.; Ismail-Beigi, S.; Capaz, R. B.; Louie, S. G. Quasiparticle and excitonic effects in the optical response of nanotubes and nanoribbons. In *Carbon Nanotubes*; Jorio, Z., Dresselhaus, G., Dresselhaus, M. S., Eds.; Springer-Verlag: Berlin and Heidelberg, 2008; pp 195−227.

NL901412X